2D Materials

RECEIVED
7 February 2015

REVISED
6 April 2015

ACCEPTED FOR PUBLICATION
20 April 2015

PUBLISHED
26 June 2015

PAPER

Controlled generation of pseudospin-mediated vortices in photonic graphene

Daohong Song[1,5], Sheng Liu[2,3,5], Vassilis Paltoglou[4,5], Daniel Gallardo[3], Liqin Tang[1], Jianlin Zhao[2], Jingjun Xu[1], Nikolaos K Efremidis[4] and Zhigang Chen[1,3]

[1] The MOE Key Laboratory of Weak-Light Nonlinear Photonics, and TEDA Applied Physics Institute and School of Physics, Nankai University, Tianjin 300457, People's Republic of China
[2] The Key Laboratory of Space Applied Physics and Chemistry, Ministry of Education and School of Science, Northwestern Polytechnical University, Xi'an 710072, People's Republic of China
[3] Department of Physics and Astronomy, San Francisco State University, San Francisco, CA 94132, USA
[4] Department of Mathematics and Applied Mathematics, University of Crete, Heraklion, 70013 Greece
[5] These authors made equal contributions.

E-mail: zhigang@sfsu.edu

Keywords: photonic graphene, pseudospin, Dirac equation, vortices

Abstract

We demonstrate controllable generation and destruction of pseudospin-mediated topological charges (vortices) in the photonic analogy of graphene—optically induced honeycomb lattices (HCLs). When only one of the two sublattices is selectively excited by the probe beams that are momentum-matched onto the Dirac points, a singly-charged optical vortex emerges in the output of the symmetric conical diffraction pattern. Furthermore, flipping of the topological charge is observed as the excitation shifts from sublattice A to sublattice B. On the other hand, when both sublattices are simultaneously excited, the conical diffraction pattern becomes highly asymmetric, accompanied by interesting phenomena related to the generation of half-integer vortices and line singularities. We present four different cases of selective excitation using two different approaches; one with three input probe beams that are momentum-matched to the three *K* valleys, and the other with only two probe beams while the Bloch modes surrounding the third valley are excited due to Bragg reflection. Our experimental results are confirmed by numerical simulation of the paraxial wave equation with a HCL potential as well as by theoretical analysis of the two-dimensional Dirac–Weyl equations directly. These studies indicate that the lattice pseudospin is not just a mathematical formality, but rather it can manifest through its angular momentum transferred to probing optical beams.

1. Introduction

Graphene, a single layer of two-dimensional (2D) carbon material, has attracted numerous interests due to its important role in understanding fundamental physics and in various potential applications in optoelectronics and photonics [1–3]. Due to its unique band gap structure, such a material exhibits exotic electron transport properties which are dramatically different from usual semiconductor materials. The conduction and valence bands are touching each other at some particular points (the so-called Dirac points) in the corner of the first Brillouin zone (BZ). In the vicinity of the Dirac points, the dispersion is linear and the dynamics of electrons is described by the Dirac equation rather than the usual Schrödinger equation, where the electrons behave as massless Dirac fermions traveling at speeds close to that of light [3]. The unique band gap structure not only results in many interesting and fundamental phenomena in graphene such as the anomalous quantum Hall effect at room temperature, Klein tunneling, and the absence of back scattering, to name just a few [1–4], but the 2D materials are also gifted with many desired optical properties such as giant optical Kerr nonlinearity [5] and broadband nonlinear optical response [6]. Since much of the underlying physics arises from the special symmetry of the graphene honeycomb lattices (HCLs), it is natural to explore the possibility of using artificial HCLs as a platform to mimic the electron transport behavior in

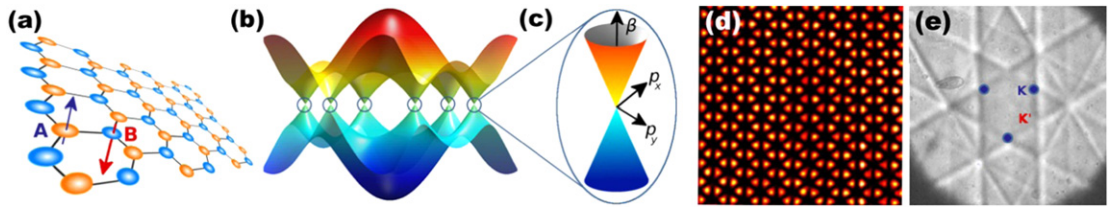

Figure 1. Schematic of the graphene honeycomb lattice (a) and the band structure (b), (c). Panels (d), (e) show experimentally generated photonic HCL and the corresponding BZ obtained with BZ spectroscopy with incoherent light. The three identical Dirac points *K* are marked with blue dots and the other three *K′* are unmarked.

carbon-based graphene. Indeed, 'artificial graphene' has been proposed and demonstrated in a number of settings, including those for electrons, photons, polaritons, surface plasmons and even cold atoms [7]. Such artificial graphene systems can be established utilizing various techniques including nanopatterning of 2D electron gases, assembling molecules on metal surfaces, trapping ultracold atoms in optical lattices, and engineering coupled micropillars in semiconductor microcavities [7–17].

The motivation for studying such artificial systems is that not only they can provide a test bed for exploring the fundamental phenomena in the graphene system, but also they can lead to new findings beyond the real carbon-based graphene. The reason is that artificial graphene systems can be easily controlled and accessed even in regimes where it is difficult or impossible for the natural graphene. In particular, photonic graphene (a honeycomb array of evanescently coupled waveguides) has proven to be a useful tool for investigating graphene physics in various optical settings [18–26]. The photonic analogy of graphene arises due to the similarity between the paraxial equation describing light propagation in HCLs and the Schrödinger equation for electrons in graphene, where the wavefunction evolving with time t is replaced by the optical field propagating along z in photonic lattices. Conveniently, the honeycomb photonic lattices can be optically induced in nonlinear photo-sensitive materials [20, 21, 23] or written in bulk fused silica glass by the femtosecond laser writing technology [23–26]. In these classical optical settings, the Bloch modes with desired momentum in photonic graphene can be selectively excited and the wavefunction including the phase can be directly measured. This has led to the direct observation of a host of interesting phenomena in photonic graphene, including defect-free Tamm-like edge states [23], strain-induced pseudomagnatic fields and photonic Landau levels [25], and photonic Floquet topological insulators [26].

Another intriguing concept arises from the sublattice degree of freedom in graphene HCLs, which is referred to as 'pseudospin'. The pseudospin has played an important role in understanding many fundamental phenomena in graphene. It is commonly believed that the introduction of pseudospin is just a mathematical analogy and the pseudospin itself is not a real physical quantity. However, a recent theoretical work has shown that the sublattice pseudospin is also a real angular momentum (AM) [27] which might be detected through its transport and optical properties [28]. So far this has not been experimentally demonstrated; although in a recent experiment visualizing electronic chirality and Berry phases in graphene systems has been realized using the photoemission with circularly polarized light [29]. Thus, it remains an open question whether it is possible or not to measure the pseudospin AM in graphene and how this could be accomplished, considering that unlike the electron spin the pseudospin cannot be detected by Stern–Gerlach-type experiments.

Quite recently, we have successfully employed the photonic graphene as a platform to study the pseudospin and its associated AM [30]. In this paper, we elaborate further on controllable generation and destruction of pseudospin-mediated topological charges (vortices) in the optically induced photonic graphene lattices. Furthermore, we report new results on asymmetric conical diffraction and other phenomena related to the generation of half-integer vortices and line singularities, due to simultaneous excitation of both sublattices. We present four different cases of selective excitation using two different approaches; one with three exciting beams which are momentum-matched to the three *K* valleys, and the other with only two exciting beams while the Bloch modes at the third valley are excited due to the Bragg reflection. We find that simultaneous excitation of both sublattices leads to asymmetric conical diffraction and generation of half-integer vortices in both spinor components, producing no net vorticity in the overall output pattern. By comparing our experimental results with numerical and theoretical analyses of the linear massless Dirac–Weyl equations, we show that the observed orbital AM of optical vortices [31] (integer or half-integer) are a direct consequence of the AM transfer from the lattice to the probe beam. Our work may provide new insights on the pseudospin related phenomena in both natural and artificial graphene systems.

As illustrated in figure 1(a), the honeycomb lattice (HCL) has a unique symmetry, and its unit cell contains two 'atoms' which are denoted as A and B. One

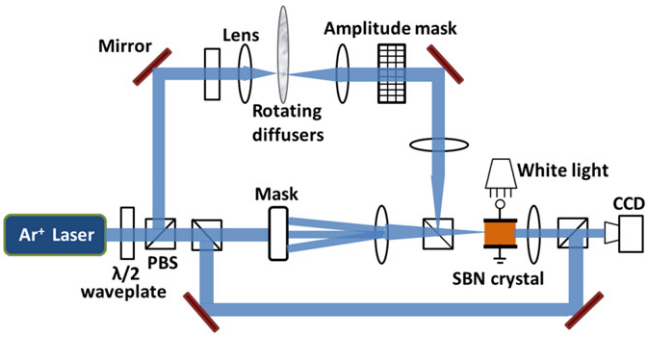

Figure 2. Schematic of the experimental setup. PBS: polarizing beam splitter. SBN: strontium barium niobate. The upper path is for optical induction of photonic HCL, the middle path is for probing into the lattice, and the bottom path is for interference measurement of the phase of the output probe beam.

can picture the HCL as being composed of two interpenetrating triangular sublattices. The band gap structure $\beta(k_x, k_y)$ plotted in figure 1(b) is calculated from the following paraxial Schrödinger-type equation describing light propagation through the lattice [20]:

$$i\frac{\partial \Psi(x, y, z)}{\partial z} = -\frac{1}{2k_0}\nabla^2\Psi(x, y, z) - \frac{k_0\Delta n(x, y)}{n_0}\Psi(x, y, z) \equiv H_0\Psi, \quad (1)$$

where Ψ is the electric field envelope of the probe beam, (x, y) are the transverse coordinates, z is the longitudinal propagation distance, k_0 is the wavenumber, n_0 is the background refractive index of the medium, and $\Delta n(x, y)$ is the induced index change forming the HCL as shown in figure 1(d), which in our experiment results from optical induction in a nonlinear photorefractive crystal as articulated below. In equation (1), H_0 is the continuous Hamiltonian of the system, whose eigenvalues are the wavenumbers along the z-direction (i.e., the propagation constant β). From figure 1(b) one can see clearly the merging of two bands at the Dirac points, where the Floquet–Bloch dispersion relation is linear (figure 1(c)). These Dirac points are located at the corners of the first BZ of the HCL, noted as K and K' in figure 1(e).

2. Optical induction of photonic graphene

In our experiment, the HCL is created by the well-known optical induction method which translates the lattice intensity pattern into the refractive index change through the nonlinearity in a photorefractive crystal [32–36]. The experimental setup is shown in figure 2. A laser beam operating at wavelength of 488 nm is divided into two parts by a polarization beam splitter: the ordinarily polarized beam passes through a rotating diffuser, and thus turned into a partially spatially incoherent beam. To generate a HCL, we use a specially designed amplitude mask to spatially modulate the otherwise uniform partially coherent beam from the diffuser. The mask is then imaged onto the front facet of the photorefractive crystal (SBN:61, with dimensions $5\times5\times20$ mm), thus creating a lattice beam, which propagates nearly invariant in the crystal. By applying either a positive or negative biased voltage, the lattice intensity pattern is transformed into the honeycomb-type periodic refractive index potential. In our experiment, we use two different induction methods to establish the honeycomb photonic lattice. In the first method we use a triangular lattice intensity pattern and apply a self-defocusing nonlinearity [20, 23], whereas in the second method we use a specially designed honeycomb amplitude mask combined with a phase mask and apply a self-focusing nonlinearity [30, 37].

The extraordinarily polarized beam from the laser is reconfigured so to be used as the probe beam. In order to selectively excite the two sublattices of photonic graphene, the probe beam is constructed by interfering either two or three broad beams, with their wavevectors pointing at one set of three Dirac points. This is realized by letting the extraordinarily polarized beam pass through a mask with three holes equally distributed on a ring, and then Fourier transformed by a circular lens. By carefully shifting the lens laterally, the position of the whole probe beam can be fine-tuned to achieve different initial excitation conditions for the HCL. The output facet of the crystal is imagined by a CCD camera. When needed, a beam splitting from the probe beam is used to form a Mach–Zehnder interferometer in order to measure the phase structure of the output from the HCL.

3. Vortex generation in photonic graphene lattices from three-beam excitation

We first discuss the case of three-beam excitation as shown in figure 3(a), for which the probe beam is constructed by interfering three beams with their wavevectors pointing (or momentum-matched) towards one set (three K valleys) of equivalent Dirac points (figures 3(a) and (c)). The intensity pattern of the probe beam exhibits a Gaussian-like truncated

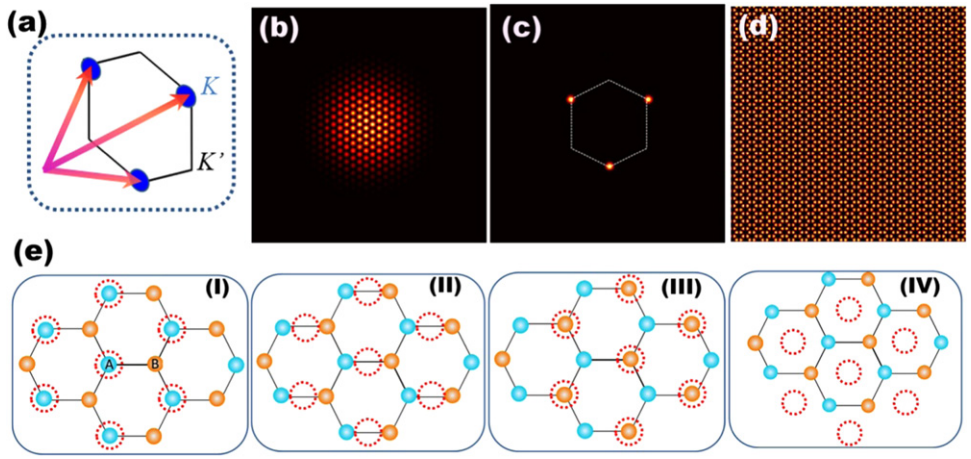

Figure 3. Illustration of three-beam excitation in the photonic HCL. (a) schematic of three-beam excitation momentum-matched to the three Dirac points *K*. (b), (c) The intensity pattern of the probe beam and its corresponding spatial spectrum (the white dashed hexagon marks the first BZ). (d) The typical HCL from simulation, and (e) four different excitation conditions, where the positions of the probe beam are marked by red dotted circles.

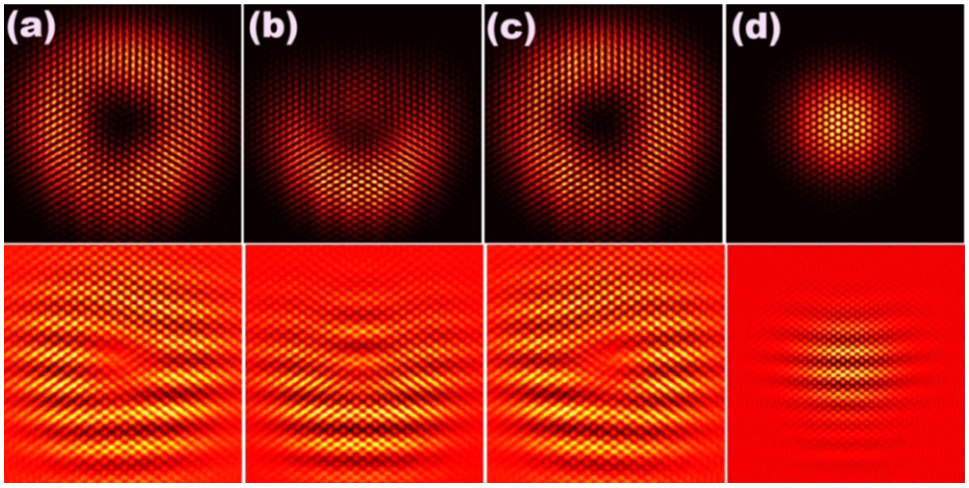

Figure 4. Simulation results of vortex generation and destruction under three-beam excitation. Panels (a)–(d) correspond to the four cases of excitation shown in figure 3(e), where the top and bottom rows show the output intensity pattern and corresponding interferograms, respectively.

triangular pattern (figure 3(b)) with its lattice spacing matching that of the honeycomb sublattice (figure 3(d)). Different pseudospin states can be excited depending on the initial position of the probe beam relative to the HCL. Here we only consider four typical settings which are schematically shown in figure 3(e) (I–IV). For case I and case III (on-site excitation), the probe beam selectively covers sublattice A and sublattice B respectively, thus only pseudospin A state or B state is excited but not both. In contrast, in case II, the probe beam sits halfway between the sites of the two sublattices, and thus both pseudospin A and B states are equally excited. As for case IV, the probe beam covers the center of the hexagonal cell (i.e., the empty site of the HCL) without overlapping/neighboring with any lattice sites, thus no excitation of any pseudospin state is expected.

Our numerical results corresponding to the above four cases of initial excitation are obtained by solving the paraxial Schrödinger-type equation (1) and are summarized in figure 4. Different pseudospin excitation conditions can be realized by simply changing the phase difference of the three interfering beams in $\boldsymbol{k}$ space. For the cases illustrated in figure 3(e), the relative phase differences are 0, $5\pi/3$, $2\pi/3$ and $4\pi/3$, respectively. The top row in figure 4 shows the output intensity pattern exiting the HCL, and the bottom row is the corresponding interference pattern with an inclined plane wave to identify the vortex generation at the output [30]. When either sublattice A or sublattice B is selectively excited (case I or III), the probe beam evolves into a symmetric ring beam with a dark core in the center, characteristic of the conical diffraction [20] (figures 4(a) and (c)). Although the output intensity patterns of the two cases are nearly identical, their

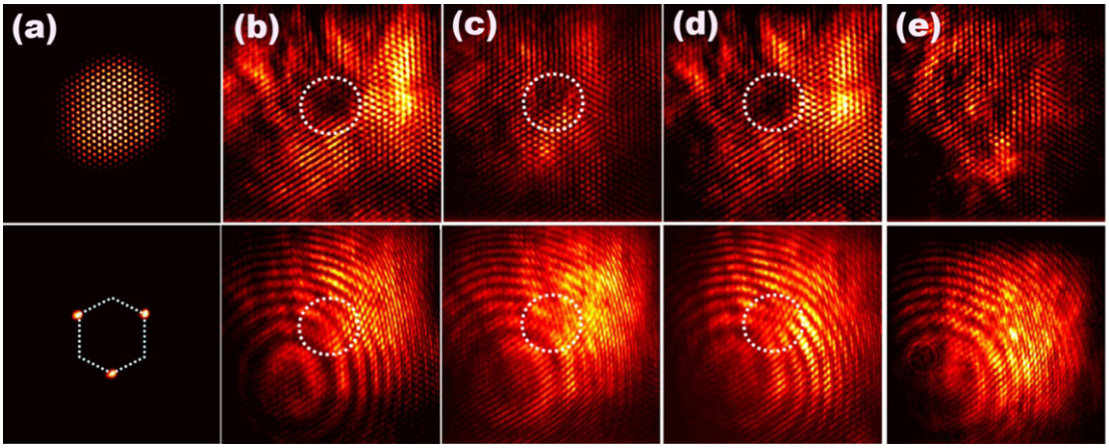

Figure 5. Experimental results of vortex generation and destruction in the photonic HCL by three-beam excitation. (a) The intensity pattern of the input beam (top) and its spatial spectrum (bottom), corresponding to figure 3(b), (c). (b)–(e) Output intensity patterns (top) and interferograms (bottom) corresponding to the four different input conditions illustrated in figure 3(e).

interferograms are quite different. Specifically, a fork-like fringe bifurcation in the center indicates that a vortex is generated, but the bifurcation direction is opposite, suggesting that the vortices generated in the two cases have opposite topological charges. On the other hand, if the probe beam is launched at off-site locations such as in case II and case IV, there is no net vorticity in the output pattern. In particular, when both sublattices are equally excited (case II), the output intensity changes to a half-ring conical diffraction pattern (figure 4(b)). The fringes in the interferogram are somewhat deformed but show no bifurcation, meaning that no net vortex is created. In case IV, not only there is no vortex identified in the output (figure 4(d)), but interestingly the output pattern is Gaussian-like rather than donut-like. This suggests that the excited modes are no longer linear band modes near the Dirac points, thus no conical diffraction occurs. For these typical simulation results, the parameters are chosen close to our experimental setting (the wavelength is $\lambda = 488$ nm, the lattice spacing is 12 μm, the propagation distance is 20 mm, and the strength of refractive index modulation is about 2×10^{-4}). These results show clearly that the vortex generation and destruction in the HCL can be controlled at ease merely by changing the input condition of the probe beam.

Next, we present our experimental results corresponding to the above four cases. The HCL is induced in the SBN crystal under self-defocusing nonlinearity [20]. The probe beam is constructed by interfering three broad Gaussian beams with their wavevectors aiming at the three Dirac points as illustrated in figure 3(a). Typical experimental results are shown in figure 5. The probe beam has a triangular lattice pattern (figure 5(a)) with a lattice period the same as that of the sublattice. The intensity of the probe beam is very low so the probe beam propagates linearly through the HCL. To selectively excite sublattice A and B, we carefully shift the focus lens transversely in real space, which is equivalent to introducing the phase differences of the three beams in $\boldsymbol{k}$-space. Just as found from simulation, when only sublattice A or sublattice B is excited, the output patterns are very similar, with an intensity dip in the center due to the conical diffraction. Opposite vortices are identified from fringe bifurcations (figures 5(b) and (d)).

In the case when both sublattices are equally excited (case II in figure 3(e)), there is no longer a fork bifurcation in the interferogram (figure 5(c)), indicating that no net vortex is generated in this case. For the off-site excitation of case IV (figure 5(e)), none of the two sublattices is excited, thus the output shows neither conical diffraction in intensity pattern nor fringe bifurcation in the interferogram. These results show that the vortex generation crucially depends on the HCL sublattice degree of freedom, i.e., the 'pseudospin', as corroborated from our theoretical analysis based on the Dirac equation [30].

4. Vortices and related phenomena from two-beam excitation

We can also selectively excite the two sublattices of the HCL by launching only two input beams instead of three, provided that the two wavevectors are momentum-matched to the two Dirac points as shown in figure 6(a). In this case, the input pattern is an interference fringe of the two beams (figure 6(b)), with a spacing appropriately selected to excite sublattice A, in between both sublattices, sublattice B, or neither (see figure 6(e) for the four cases). Note that, because the input beam is now more like a one-dimensional lattice rather than 2D triangular lattice, there is no perfect equivalence between the excitation conditions in figure 6(e) and those in figure 3(e). Nevertheless, as we shall show below, there is a striking similarity in the

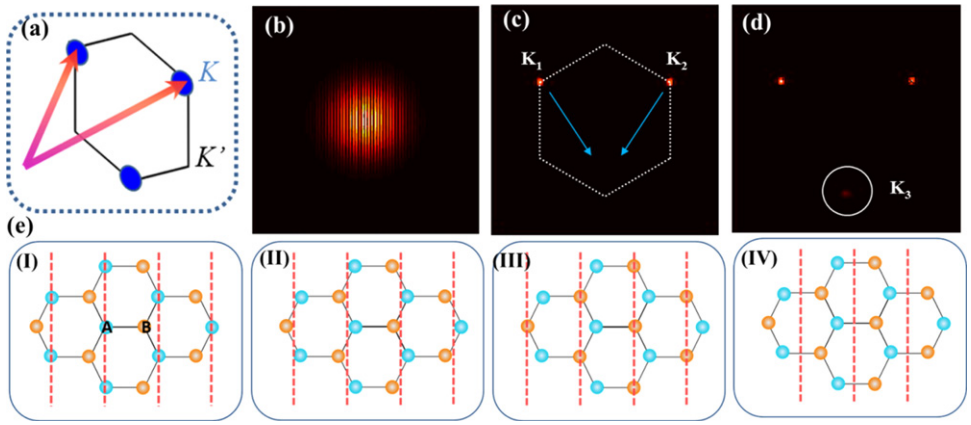

Figure 6. Illustration of two-beam excitation in the photonic HCL. (a) Schematic of the two-beam excitation momentum-matched to the two Dirac points. (b) Input probe beam and (c) its spectrum at K_1 and K_2. (d) Output spectrum where a new spectral component generated from Bragg reflection at K_3 is circled. (e) Four different excitation conditions, where the positions of the probe beam are marked by red dashed lines.

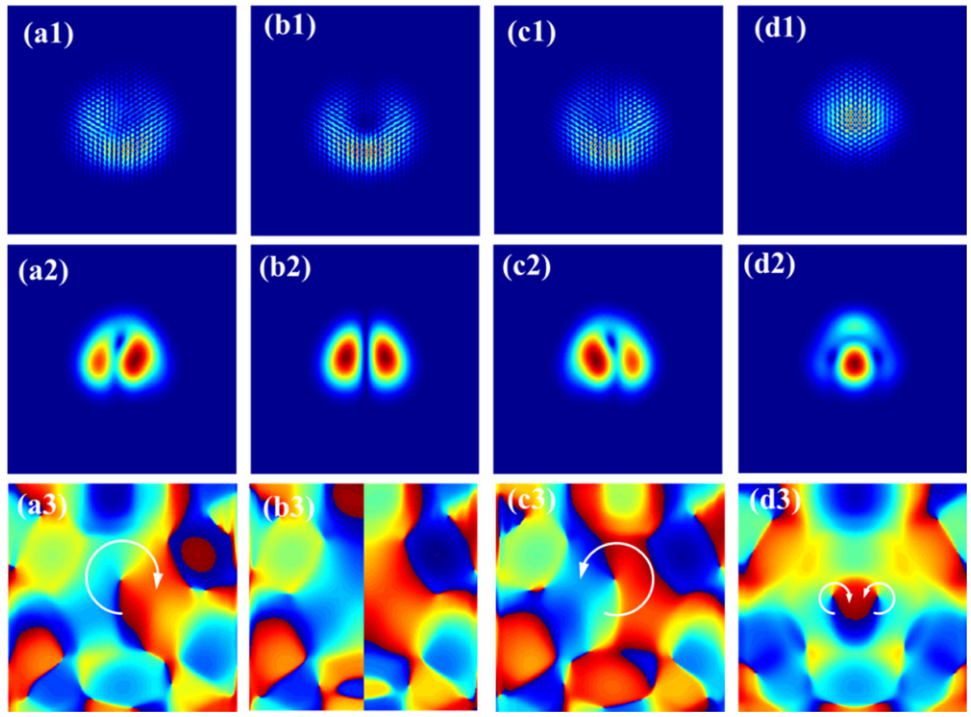

Figure 7. Numerical results from two-beam excitation in the photonic HCL. (a)–(d) Output corresponding to cases I–IV in figure 6. Top row: diffraction pattern of the input beam; middle and bottom rows: intensity and phase distributions of the far field extracted from the Bragg-reflected spectral component at the Dirac point K_3.

vortex generation, in the cases I and III (i.e., only one of the two sublattices is excited).

For the two-beam excitation in the HCL, the two components are momentum-matched to the Dirac points K_1 and K_2 (figure 6(c)) and experience the Bragg reflections from the lattice. Thus, a new spectrum component emerges at the third Dirac point K_3 (figure 6(d)). Since the formation of Bloch modes can be attributed to the Bragg reflection, it is reasonable to consider that the new component should contain the information of the excited modes. Thus, we extract this Bragg-reflected K_3 component and make an inverse Fourier transform from the momentum $\boldsymbol{k}$-space back to the real space, where the intensity and phase of the excited mode can be better visualized.

We first present the numerical simulations for the above described four different cases. The results are shown in figure 7, where the first row shows the output diffraction pattern of the input beam, while the second and third rows are the intensity and phase distributions extracted from the Bragg-reflected spectral component, respectively. For cases I or III, only sublattice A or B is excited, and thus the output intensity still displays a conical diffraction pattern. More importantly,

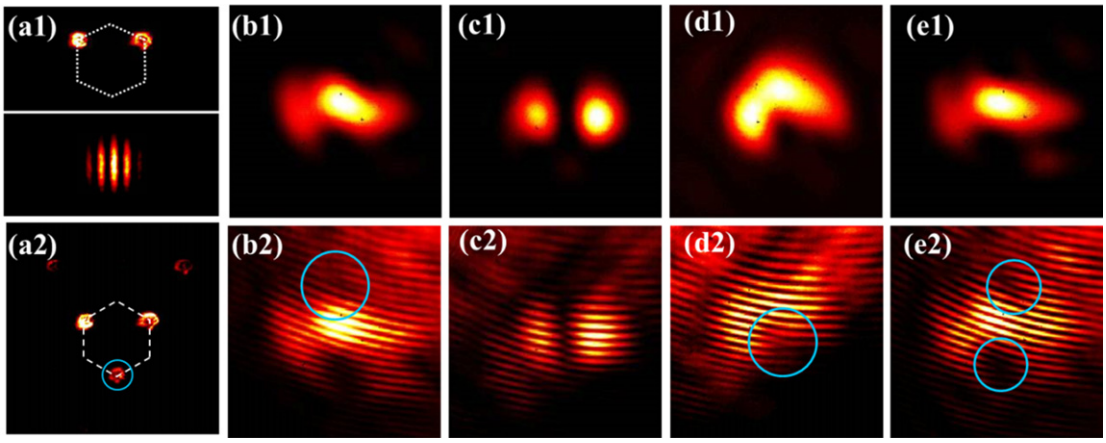

Figure 8. Experimental results from two-beam excitation in the photonic HCL. (a1) Input *k*-space spectrum (top) and intensity (bottom) of the probe beam; (a2) output spectrum where a new spectral component generated from Bragg reflection at K_3 is circled; (b)–(e) Output far-field intensity patterns (top) and interferograms (bottom) corresponding to figures 7(a)–(d), where the blue circles mark the locations of the phase singularities.

the spiral phase structure shows the generation of opposite vorticities (figures 7(a) and (c)), illustrating again the honeycomb sublattice degree of freedom, i.e., the pseudsopin. When the input fringe pattern is launched at the narrow gaps between the two sublattices A and B (case II in figure 6(e)), the output field again displays a half-ring conical diffraction pattern (figure 7(b)). Interestingly, the far-field pattern from the K_3 component resembles a dipole structure. As for case IV, the input fringe is launched at the widest gaps between the sublattice sites (case IV in figure 6(e)), and there are two vortices with opposite topological charges emerging at the far field (figure 7(d)). This vortex-pair mode must have arisen from a higher band rather than from the Dirac points, simply because the output intensity now exhibits no conical diffraction.

To experimentally observe the pseudospin-mediated vortex generation shown above, we employ two interfering beams as illustrated in figure 6(a), whose interference pattern and Fourier spectrum are displayed in figure 8(a). As expected, a new spectrum component at the third Dirac point K_3 emerges due to the Bragg reflection. To extract this component, a low-pass filter is used together with a lens for inverse Fourier transform. The far-field intensity pattern is shown in the top panels of figure 8. By interfering with another plane wave, the phase of this output field can be analyzed (see the bottom panels of figure 8). To change the excitation from case I to case IV, we shift the lattice-inducing beam slightly in the lateral direction. It can be seen that the experimental results agree well with the numerical ones: by selective excitation of the HCL, the far-field structure of the K_3-point component undergoes a transition from a vortex of positive charge, to a dipole, to a vortex of negative charge, and finally to a vortex-pair with no net vorticity.

5. Theoretical analysis from the Dirac system

Our numerical and experimental results clearly show that the AM of the probe is not conserved when only one sublattice is excited due to the fact that a vortex (with orbital AM [31]) is generated at the output after propagating through the HCL. To better understand the underlying physics of this intriguing phenomenon, we analyze directly the Dirac–Weyl equations. In fact, the Schrödinger equation with a honeycomb potential can be simplified into the 2D Dirac-like equations around the Dirac points [22, 30, 38, 39]. Applying the coupled-mode theory (under the tight-binding approximation) to equation (1), one can obtain a two-band simplified description of the paraxial model. In the continuous limit and for excitations near the Dirac points, the coupled mode equation turns into the linear Dirac equations typically used for describing massless Dirac particles in graphene:

$$\begin{aligned} \mathrm{i}\partial_z\psi_A + \left(\partial_x - \mathrm{i}\mu\partial_y\right)\psi_B = 0, \\ \mathrm{i}\partial_z\psi_B - \left(\partial_x + \mathrm{i}\mu\partial_y\right)\psi_A = 0, \end{aligned} \tag{2}$$

where $\mu = (-1)^m = \pm 1$, and $m = 0, \ldots, 5$ is the index of the six Dirac points shown in figure 1(e). The associated Hamiltonian can be written as $H = \sigma_y p_x - \kappa\sigma_x p_y$, where $p = (p_x, p_y)$ is the Bloch momentum measured from the Dirac points, $\boldsymbol{\sigma} = (\sigma_x, \sigma_y)$ are the Pauli matrices. Thus, an optical beam with Bloch momentum at the close vicinity of Dirac points is governed by the Dirac–Weyl equation, akin to massless Dirac Fermions in graphene. The optical wave in the spatially separated sublattice sites (marked as A and B in figure 1(a)) is modeled by the two-component spinor function $\psi = (\psi_A, \psi_B)$. As such, the sublattice A and B states play the same role as those of electron spin, thus typically referred to as the 'pseudospin'.

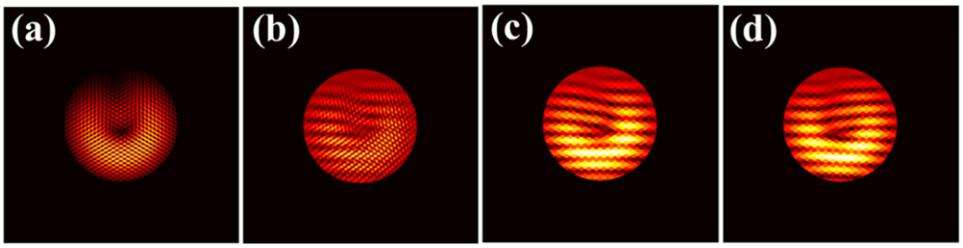

Figure 9. Theoretical results for the case when both sublattices are equally excited. (a) Output field amplitude. (b) Phase interferogram of the optical wave. Panels (c), (d) show the interferograms of the same output field when sublattice A and B are isolated.

Detailed theoretical analysis of the above Dirac system that leads to the understanding of the pseudospin AM, by breaking the sublattice degeneracy in a photonic HCL, is presented in [30] and the accompanying supplementary information. The main conclusion is that, by selective excitation of only one of the two sublattices (cases I and III), symmetric conical diffraction and the generation of singly charged vortices in otherwise vortex-free beams (probe) are observed due to the transfer from the lattice pseudospin to the orbital AM of the probe. Here, we focus on the understanding of the case of simultaneous excitation of both sublattices (case II) near the Dirac points that leads to surprisingly different behavior.

In case II where both of the sublattices are equally excited, we can analyze the behavior of the system via superimposing the dynamics in which sublattice A and sublattice B are solely excited at the input. As a result of the excitation of sublattice A, a vortex with vorticity −1 is generated in sublattice B. In addition, due to the equal excitation of sublattice B, a vortex is generated in sublattice A with vorticity +1. As revealed by the steepest descent asymptotics (see the supplementary material of [30]), when exciting a single spinor component with a Gaussian beam, asymptotically for relatively large propagation distances, both of the sublattices are associated with the same amplitude. As a result, the output wave on sublattice A in this case consists of a vortex beam with vorticity +1 and an additional beam without vorticity; both of which have almost the same ring amplitude $\Psi_0(r, z)$, where $r = (x^2 + y^2)^{1/2}$ is the radial coordinate. Thus, the asymptotic form of the total field on sublattice A becomes $\Psi_A = 2e^{i\phi/2}\Psi_0(r, z)\cos(\phi/2)$. The amplitude profile now has the semi-ring structure that explains the asymmetric conical diffraction pattern discussed before. We note that, unexpectedly, in this case the vortex in sublattice A actually has a semi-integer vorticity +1/2. In addition a line singularity is obtained where the beam acquires an additional π phase difference [40]. Following similar arguments we can obtain the field on sublattice B as $\Psi_B = 2e^{-i\phi/2}\Psi_0(r, z)\cos(\phi/2)$. Thus we can see that there are two semi-vortices generated in the two sublattices A and B with opposite semi-integer vorticities +1/2 and −1/2 along with two line singularities. Overall, this leads to no net vorticity in the output. These asymptotic results are in excellent agreement with the numerical results and the experimental observations. As we can see in figure 9(a), the field amplitude exhibits the predicted characteristic semi-ring structure and becomes zero along the positive y-axis. In addition, the interferogram in figure 9(b) clearly shows the π-phase line-singularity. By selectively isolating sublattices A and B, the semi-vortex structure with opposite vorticities (+1/2 and −1/2) is revealed (figures 9(c) and (d)). As for the Case IV, the Gaussian-type amplitude profile at the output is an indication that we are not close to the Dirac cone. In this case, the input beam could excite modes in the vicinity of the BZ center (Γ point) or higher band modes but with no net vorticity at the output. These results agree well with our previous simulation results from the Schrödinger equation and with our experimental results.

6. Discussion and summary

Before closing, a few issues merit further discussion. Firstly, we want to clarify why the two-beam excitation results (figures 7 and 8) show a dipole-like pattern for equal excitation (case II), but not a half-vortex pattern as expected from theory (figure 9). One might understand this intuitively: the key is the filtering at K_3 point (figure 6(d)). For the two-beam excitation, the conical diffraction output indeed resembles a half-vortex (figure 7(b1)). After extracting the K_3 component, the output looks more like a dipole pattern. According to the theory in section 5, the output field with excitation of only one sublattice, e.g. sublattice A, contains two parts: one is a vortex with vorticity −1 in sublattice B that comes from the Bragg reflection; the other is the remaining original field in sublattice A without vorticity. Then the semi-vortex emerges with excitation of both sublattices simultaneously as explained above. However, in our two-beam excitation approach, when extracting K_3 component which comes from the Bragg reflection, the remaining original field is removed, and thus it should be a full (integer) vortex. Therefore, when exciting both sublattices, the extracted K_3 component contains both the

+1 and −1 vortices from sublattices A and B, respectively, leading to a dipole-like intensity pattern due to the superposition.

Secondly, we want to emphasize that in all our experiments we excite the same set of Dirac points, i.e. the same *K* valleys, with the topological charge of the vortex depending on the sublattice degree freedom on the same valley. Studies of the valley degree of freedom [41] in our optical setting of photonic graphene are certainly interesting for our future work. As predicted theoretically, the pseudospin should be a real AM, since the orbital AM itself is not conserved in the Dirac equation [27]. The vortex AM observed in our experiments must origin from the AM transfer from the initial pseudospin in the HCL. We also want to mention that, recently, relevant theoretical work has also shown that pseudospin in the Lieb lattice is not a mathematic formality but has real physical effects [42]. Thus, it is reasonable to believe that the pseudospin-mediated vortex phenomena will also appear in Lieb lattices, Kagomé lattices [43] and other lattice structures or 2D material systems [44].

In summary, we have demonstrated that the pseudospin-mediated vortex generation can be controlled in photonic graphene simply by selective excitation of the two HCL sublattices. The vortex generation can be observed only when one of the two sublattices is excited, and the topological charge of the vortex depends on the sublattice degree of freedom. When both sublattices of photonic graphene are equally excited near the Dirac points, asymmetric conical diffraction is observed, accompanied by generation of pseudospin-mediated non-integer phase singularities. The results obtained in our optical system can also be applied to other natural graphene and artificial graphene systems. Moreover, our work also reveals a new physical mechanism for generating and controlling optical beams with orbital AM which may find applications in photonics.

Acknowledgement

This research is supported by the 973 programs (2013CB632703, 2013CB328702, 2012CB921900) and the National Natural Science Foundation (11304165, 61205001), PCSIRT (IRT0149) and 111 Project (No. B07013) in China and by the US National Science Foundation and Air Force Office of Scientific Research. VP and NKE are supported by the action 'ARISTEIA' in the context of the Operational Programme 'Education and Lifelong Learning' that is co-funded by the European Social Fund and National Resources. We thank M Ablowitz and Y Zhu for discussion and assistance.

References

[1] Novoselov K, Geim A K, Morozov S, Jiang D, Katsnelson M, Grigorieva I, Dubonos S and Firsov A 2005 Two-dimensional gas of massless Dirac fermions in graphene *Nature* **438** 197–200
[2] Zhang Y, Tan Y-W, Stormer H L and Kim P 2005 Experimental observation of the quantum Hall effect and Berry's phase in graphene *Nature* **438** 201–4
[3] Castro Neto A H, Guinea F, Peres NMR, Novoselov K S and Geim A K 2009 The electronic properties of graphene *Rev. Mod. Phys.* **81** 109–62
[4] Katsnelson M, Novoselov K and Geim A 2006 Chiral tunnelling and the Klein paradox in graphene *Nat. Phys.* **2** 620–5
[5] Hendry E, Hale P J, Moger J, Savchenko A K and Mikhailov S A 2010 Coherent nonlinear optical response of graphene *Phys. Rev. Lett.* **105** 097401
[6] Bonaccorso F, Sun Z, Hasan T and Ferrari A C 2010 Graphene photonics and optoelectronics *Nat. Photon.* **4** 611–22
[7] Polini M, Guinea F, Lewenstein M, Manoharan H C and Pellegrini V 2013 Artificial honeycomb lattices for electrons, atoms and photons *Nat. Nanotechnol.* **8** 625–33
[8] Singha A *et al* 2011 Two-dimensional mott-hubbard electrons in an artificial honeycomb lattice *Science* **332** 1176–9
[9] Gibertini M, Singha A, Pellegrini V, Polini M, Vignale G, Pinczuk A, Pfeiffer L N and West K W 2009 Engineering artificial graphene in a two-dimensional electron gas *Phys. Rev.* B **79** 241406
[10] Gomes K K, Mar W, Ko W, Guinea F and Manoharan H C 2012 Designer Dirac fermions and topological phases in molecular graphene *Nature* **483** 306–10
[11] Tarruell L, Greif D, Uehlinger T, Jotzu G and Esslinger T 2012 Creating, moving and merging Dirac points with a Fermi gas in a tunable honeycomb lattice *Nature* **483** 302–5
[12] Soltan-Panahi P, Struck J, Hauke P, Bick A, Plenkers W, Meineke G, Becker C, Windpassinger P, Lewenstein M and Sengstock K 2011 Multi-component quantum gases in spin-dependent hexagonal lattices *Nat. Phys.* **7** 434–40
[13] Zhang Y, Wu Z, Belic M R, Zheng H, Wang Z, Xiao M and Zhang Y 2015 Photonic Floquet topological insulator in an atomic ensemble *Laser Photon. Rev.* doi:10.1002/lpor.201400428
[14] Weick G, Woollacott C, Barnes W L, Hess O and Mariani E 2013 Dirac-like plasmons in honeycomb lattices of metallic nanoparticles *Phys. Rev. Lett.* **110** 106801
[15] Park C-H and Louie S G 2009 Making massless Dirac fermions from a patterned two-dimensional electron gas *Nano Lett.* **9** 1793–7
[16] Jacqmin T, Carusotto I, Sagnes I, Abbarchi M, Solnyshkov D D, Malpuech G, Galopin E, Lemaître A, Bloch J and Amo A 2014 Direct observation of Dirac cones and a flatband in a honeycomb lattice for polaritons *Phys. Rev. Lett.* **112** 116402
[17] Uehlinger T, Jotzu G, Messer M, Greif D, Hofstetter W, Bissbort U and Esslinger T 2013 Artificial graphene with tunable interactions *Phys. Rev. Lett.* **111** 185307
[18] Sepkhanov R A, Bazaliy Y B and Beenakker C W J 2007 Extremal transmission at the Dirac point of a photonic band structure *Phys. Rev.* A **75** 063813
[19] Ochiai T and Onoda M 2009 Photonic analog of graphene model and its extension: Dirac cone, symmetry, and edge states *Phys. Rev.* B **80** 155103
[20] Peleg O, Bartal G, Freedman B, Manela O, Segev M and Christodoulides D N 2007 Conical diffraction and gap solitons in honeycomb photonic lattices *Phys. Rev. Lett.* **98** 103901
[21] Bahat-Treidel O, Peleg O, Grobman M, Shapira N, Segev M and Pereg-Barnea T 2010 Klein tunneling in deformed honeycomb lattices *Phys. Rev. Lett.* **104** 063901
[22] Fefferman C and Weinstein M 2012 Honeycomb lattice potentials and Dirac points *J. Am. Math. Soc.* **25** 1169–220
[23] Plotnik Y *et al* 2014 Observation of unconventional edge states in 'photonic graphene' *Nat. Mater.* **13** 57–62

[24] Rechtsman M C, Plotnik Y, Zeuner J M, Song D, Chen Z, Szameit A and Segev M 2013 Topological creation and destruction of edge states in photonic graphene *Phys. Rev. Lett.* **111** 103901
[25] Rechtsman M C, Zeuner J M, Tünnermann A, Nolte S, Segev M and Szameit A 2013 Strain-induced pseudomagnetic field and photonic Landau levels in dielectric structures *Nat. Photon.* **7** 153–8
[26] Rechtsman M C, Zeuner J M, Plotnik Y, Lumer Y, Podolsky D, Dreisow F, Nolte S, Segev M and Szameit A 2013 Photonic floquet topological insulators *Nature* **496** 196–200
[27] Mecklenburg M and Regan B C 2011 Spin and the honeycomb lattice: lessons from graphene *Phys. Rev. Lett.* **106** 116803
[28] Trushin M and Schliemann J 2011 Pseudospin in optical and transport properties of graphene *Phys. Rev. Lett.* **107** 156801
[29] Liu Y, Bian G, Miller T and Chiang T C 2011 Visualizing electronic chirality and berry phases in graphene systems using photoemission with circularly polarized light *Phys. Rev. Lett.* **107** 166803
[30] Song D, Paltoglou V, Liu S, Zhu Y, Gallardo D, Tang L, Xu J, Ablowitz M, Efremidis N K and Chen Z 2015 Unveiling pseudospin and angular momentum in photonic graphene *Nat. Commun.* **6** 6272
[31] Allen L, Beijersbergen M W, Spreeuw R J C and Woerdman J P 1992 Orbital angular momentum of light and the transformation of Laguerre–Gaussian laser modes *Phys. Rev.* A **45** 8185–9
[32] Efremidis N K, Sears S, Christodoulides D N, Fleischer J W and Segev M 2002 Discrete solitons in photorefractive optically induced photonic lattices *Phys. Rev.* E **66** 046602
[33] Fleischer J W, Segev M, Efremidis N K and Christodoulides D N 2003 Observation of two-dimensional discrete solitons in optically induced nonlinear photonic lattices *Nature* **422** 147–50
[34] Neshev D, Ostrovskaya E, Kivshar Y and Krolikowski W 2003 Spatial solitons in optically induced gratings *Opt. Lett.* **28** 710–2
[35] Martin H, Eugenieva E D, Chen Z and Christodoulides D N 2004 Discrete solitons and soliton-induced dislocations in partially coherent photonic lattices *Phys. Rev. Lett.* **92** 123902
[36] Chen Z, Segev M and Christodoulides D N 2012 Optical spatial solitons: historical overview and recent advances *Rep. Prog. Phys.* **75** 086401
[37] Gao Y, Song D, Chu S and Chen Z 2014 Artificial graphene and related photonic lattices generated with a simple method *IEEE Photon. J.* **6** 1–6
[38] Ablowitz M J, Nixon S D and Zhu Y 2009 Conical diffraction in honeycomb lattices *Phys. Rev.* A **79** 053830
[39] Paltoglou V, Chen Z and Efremidis N K 2015 Composite multi-vortex diffraction-free beams and van Hove singularities in honeycomb lattices *Opt. Lett.* **40** 1037–40
[40] Jonathan L, Eric Y and Miles J P 2004 Observation of the vortex structure of a non-integer vortex beam *New J. Phys.* **6** 71
[41] Xiao D, Yao W and Niu Q 2007 Valley-contrasting physics in graphene: magnetic moment and topological transport *Phys. Rev. Lett.* **99** 236809
[42] Leykam D, Bahat-Treidel O and Desyatnikov A S 2012 Pseudospin and nonlinear conical diffraction in Lieb lattices *Phys. Rev.* A **86** 031805
[43] Atwood J L 2002 Kagome lattice: a molecular toolkit for magnetism *Nat. Mater.* **1** 91–2
[44] Mas-Balleste R, Gomez-Navarro C, Gomez-Herrero J and Zamora F 2011 2D materials: to graphene and beyond *Nanoscale* **3** 20–30